Numer. Math. Theor. Meth. Appl.
doi: 10.4208/nmtma.2014.1306si

Vol. **7**, No. 4, pp. 512-523
November 2014

Modeling the Sedimentation of Red Blood Cells in Flow under Strong External Magnetic Body Force Using a Lattice Boltzmann Fictitious Domain Method

Xing Shi[1] and Guang Lin[2,3,*]

[1] *School of Aeronautics and Aerospace, Zhejiang University, Hangzhou, 310027, P.R. China.*
[2] *Department of Mathematics, School of Mechanical Engineering, Purdue University, West Lafayette, IN 47907, USA.*
[3] *Computational Mathematics Group, Fundamental and Computational Sciences Directorate, Pacific Northwest National Laboratory, 902 Battelle Blvd., P.O. Box 999, WA 99352, USA.*

Received 1 October 2013; Accepted 11 March 2014

Available online 11 November 2014

Abstract. Experimental observations show that a strong magnetic field has a dramatic influence on the sedimentation of RBCs, which motivates us to model the sedimentation of red blood cell (RBC) under strong external magnetic body force. To model the sedimentation of a RBC in a square duct and a circular pipe, a recently developed technique derived from the lattice Boltzmann and the distributed Lagrange multiplier/fictitious domain methods (LBM-DLM/FD) is extended to employ the mesoscopic network model for simulations of the sedimentation of a RBC in flow. The flow is simulated by the LBM with a strong magnetic body force, while the network model is used for modeling RBC deformation. The fluid-RBC interactions are enforced by the Lagrange multiplier. The sedimentation of RBC in a square duct and a circular pipe is simulated, which demonstrates the developed method's capability to model the sedimentation of RBCs in various flows. Numerical results illustrate that the terminal settling velocity increases incrementally with the exerted body force. The deformation of RBC has a significant effect on the terminal settling velocity due to the change in the frontal area. The larger the exerted force, the smaller the frontal area and the larger the RBC deformation become. Additionally, the wall effect on the motion and deformation of RBC is also investigated.

AMS subject classifications: 76Z05, 92C35, 92C10

Key words: Sediment, erythrocyte, fictitious domain method, lattice Boltzmann method, flow-structure interaction, red blood cell.

*Corresponding author. *Email address:* guanglin@purdue.edu (G. Lin)

1. Introduction

Red blood cell (RBC) containing haemoglobin was revealed to be susceptible to magnetic fields [1,2]. The behavior of red blood cells will be greatly affected by strong external magnetic force. Many cardiovascular diseases, such as artherosclerotic disease, strokes, heart attacks, and so on, are related to high blood viscosity. Furthermore, blood viscosity is the key parameter that modulates hemodynamic forces such as shear stress and strain in the vessels, as well as blood pressure. Additionally, hyperviscosity may cause the pre-inflammatory injury that triggers endothelial dysfunction and a cascade of events that result in the hardening and thickening of arterial walls. Hence, reduction of the high blood viscosity is a direct way to reduce the risk of having these diseases or alleviate the potential hardening and thickening of arterial walls. One of the possible means is to impose strong magnetic fields parallel to the blood flow direction. The apparent viscosity would be reduced by 20%$\sim$30% at a magnetic field pulse of 1.3T lasting around 1 min where the RBCs is aggregated along the field direction to form short chain at the microscopic level [3]. Another application of magnetic field is the separation of red blood cell from the blood [2]. High gradient magnetic field is adopted in the process of separation based on the fact that the paramagnetic properties of the reduced haemoglbin [2]. The advantage of using magnetic separation lies in that this magnetic separation is a physical process without the use of additives which may pollute the blood. Thus, it is critical to study the effect of the magnetic fields on the behavior of RBC in fluid flow.

Recently, numerical simulations of red blood cells attract increasing attention because of the important role of RBCs in blood circulation. Simulations of individual RBCs provide a down-to-cell approach to study blood flow. Pioneering and fundamental work conducted by Fung [4], Fung and Zweifach [5], Evans [6], Skalak and Branemark [7], Secomb et al. [8], etc., explored the structure and properties of a RBC membrane and established mathematical RBC models. It is well known that the RBC has no nucleus, and both the cytosol and the plasma are Newtonian fluids. A RBC membrane is composed of a phospholipid bilayer supported by protein skeleton resistant to extension and compression. During the deformation in blood flow, RBCs roughly maintain their surface area and volume. Motion and deformation RBCs in fluid flow are a typical fluid-structure interaction problem where the sub-problems to be solved included the fluid flow, the RBC deformation and motion, the coupling of fluid and RBC interaction and the constitutive equations and models for the fluid and RBC. Many methods were proposed for the flow-structure interactions [4, 8, 10–18]. In this paper, the lattice Boltzmann method (LBM) [19, 20] is employed to solve the flow. The RBC is modeled as a closed membrane filled with cytosol and immersed in plasma. A coarse-grained mesoscopic method developed by Fedosov et al. [11] is used to represent the properties of a RBC membrane, where the spring network model representing the spectrin cytoskeleton of a RBC can be carried out with a coarse mesh to improve computational efficiency. The coupling of flow-RBC interactions is handled by the distributed-Lagrange-multiplier (DLM) based fictitious-domain method, to avoid

the remeshing procedure when the flow-RBC interface is updated. The advantage of the developed method is the reduction of the complexity of the algorithm and the cost of computation is greatly reduced. Additionally, the developed method is more suitable for simulating large deformation of RBC. Experimental observations [1–3] show that a strong magnetic field has a dramatic influence on the sedimentation of RBCs, which motivates us to model the sedimentation of RBCs under strong external magnetic body force in this work. As an initial step to the study of the effect of magnetic field, the magnetic force is considered as a uniform body force exerted on a RBC [22]. In this paper, simulations of the sedimentation of a single RBC in a square duct and a circular pipe under strong magnetic body force are performed by the LBM-DLM/FD method [18, 21] with the developed mesoscopic membrane model [11].

The paper is organized as follows: Section 2 outlines the mathematical formulation. In Section 3, two numerical tests, including the sedimentation of RBC in a square duct and a circular pipe, are performed. Section 4 presents a brief conclusion.

2. Mathematical formulation

2.1. LBM-DLM/FD method

In this paper, the sedimentation of a RBC in a duct flow is simulated by the developed LBM-DLM/FD method [18, 21], which is a FDM within the LBM framework. In this method, the computational domain includes both the fluid and solid domains, and the flow-structure coupling is handled by the Lagrange multiplier method. The merit of LBM-DLM/FD method is that no re-meshing procedure is needed when the flow-structure interface changes, making it possible to deal with large deformation of structure. The equations in the LBM-DLM/FD method include equations of the fluid subdomain, equations of the solid subdomain, and equations to constrain fluid and solid motion. The fluid-structure coupling on the fluid-structure interface is also imposed by the Lagrange multiplier, and the information exchange is implemented by interpolation.

The fluid domain is solved by the lattice Boltzmann equations (LBEs). The form of LBEs used here includes the DLM, $\boldsymbol{\lambda}$, in the body force term under the incompressible limit [19, 20]:

$$f_i(t+\delta_t, \mathbf{x}+\mathbf{e}_i\delta_t) = f_i(t,\mathbf{x}) - \frac{1}{\tau}(f_i - f_i^{eq}) + \frac{w_i\delta_t}{c_s^2}\left[(\boldsymbol{\lambda}+\rho_f\mathbf{f}_f)\cdot\mathbf{e}_i\right], \tag{2.1}$$

where f_i is the single-particle distribution function in the i-direction of the microscopic velocity, δ_t denotes the time scale. $\mathbf{f}_f$ is the external force acting on the fluid. w_i is the corresponding weighting factor of the density distribution in each velocity direction. τ is the relaxation time associated with the kinematic viscosity of the fluid and reflects the relaxation rate to the local equilibrium distribution f_i^{eq}. The macroscopic fluid velocity

$\mathbf{u}_f$ and mass density ρ_f are obtained from the distribution functions as follows [19]:

$$\rho_f = \sum_i f_i, \quad \rho_f \mathbf{u}_f = \sum_i f_i \mathbf{e}_i. \tag{2.2}$$

The solid or structure motion is controlled by following equation in weak form [16]:

$$\int_{\Omega_s} \left((\rho_s - \rho_f) \frac{d\mathbf{u}_s}{dt} - (\rho_s \mathbf{f}_s - \rho_f \mathbf{f}_f) \right) \cdot \boldsymbol{\varphi}_s d\Omega_s - \int_{\Omega_s} [\nabla \cdot (\boldsymbol{\sigma}_s - \boldsymbol{\sigma}_f)] \cdot \boldsymbol{\varphi}_s d\Omega_s + \int_{\Omega_s} \boldsymbol{\lambda} \cdot \boldsymbol{\varphi}_s d\Omega_s = 0, \tag{2.3}$$

where $\mathbf{u}$ is the velocity, ρ is the mass density, $\mathbf{f}$ is the body force, and $\boldsymbol{\sigma}$ is the stress. The subscripts f and s correspond to the flow and structure variables, respectively. $\boldsymbol{\varphi}_s$ is the weighting function. The RBC deformation in flow always can be assumed to be in a quasi-equilibrium process. Hence, the acceleration term in the preceding equation can be ignored. The cell is divided into two parts by the membrane: the inner and outer parts. In this paper, the external magnetic force is treated as the constant body force acting on the whole cell. Thus, in the inner part, $\mathbf{f}_f = \mathbf{f}_{mag}$, and, in the outer part, $\mathbf{f}_f = 0$. In every time step, the property at the grid points located in and out of a cell is updated to determine whether the external body force should be imposed.

2.2. Red blood cell model

The coarse-grained model of RBC membrane, first proposed by Boey et al. [9] and further developed by Li et al. [10], and Fedosov et al. [11], is employed here. The membrane surface is triangulated with N nodes, E edges, and T triangles. The total energy of the system is defined as:

$$V(\mathbf{x}_n) = V_{in-plane} + V_{bending} + V_{surface} + V_{volume}, \tag{2.4}$$

where $\mathbf{x}_n$ represents the vertex coordinates and the in-plane energy is expressed by:

$$V_{in-plane} = \sum_{all\,edges} V_{wlc} + \sum_{all\,edges} V_p. \tag{2.5}$$

Each edge in the network is a spring defined by two potentials — a wormlike chain with the energy V_{wlc} and a repulsive potential with the energy V_p. $V_{bending}$ is the membrane bending energy. The surface and volume terms, $V_{surface}$ and V_{volume} respectively, are used to constrain the variation of the surface area and volume to be small. More details regarding individual energy can be found in [11]. Finally, the nodal forces are derived from the total energy as follows:

$$F_n^{membrane} = -\frac{\partial V(\mathbf{x}_n)}{\partial \mathbf{x}_n}. \tag{2.6}$$

3. Numerical simulations and discussion

3.1. Modeling the sedimentation of a RBC in a square duct

Fig. 1 shows the flow domain setup: a RBC with the diameter d and length l is placed on the centerline of a square duct with the width of W. The top and bottom are set as periodic boundaries, while the others are set as wall boundaries. An external body force is applied on the cell along the vertical direction. The cell membrane is decomposed into 996 triangular elements. The shear and bending moduli of a RBC are set to 6.3 $\mu m/m$ and $2.4 \times 10^{-19} N \cdot m$, respectively. The equivalent radius of a RBC is adopted as the characteristic length:

$$a = (3V/4\pi)^{\frac{1}{3}}, \tag{3.1}$$

where V is the cells volume. In this paper, the volume of a healthy RBC is assumed to be 93 μm^3 [1]. Hence, our result is $a = 2.82\ \mu m$. Then, under the creeping flow condition, the terminal settling velocity of a sphere with the radius a in an infinite flow field and used as a characteristic velocity is given as:

$$U_0 = \frac{F}{6\pi a \mu_f}, \tag{3.2}$$

where F is the external body force and μ_f is the fluid viscosity. The initial diameter of RBC is 8.8 μm and is equal to 48 δ_x, where δ_x denotes the lattice spacing in the lattice Boltzmann method. The relaxation time, τ, in the lattice Boltzmann method related to the kinematic viscosity of the fluid is set to 0.98, which reflects the relaxation rate to the local equilibrium distribution. According to [22], the external force used here is on the order of $10^{-10}\ N$.

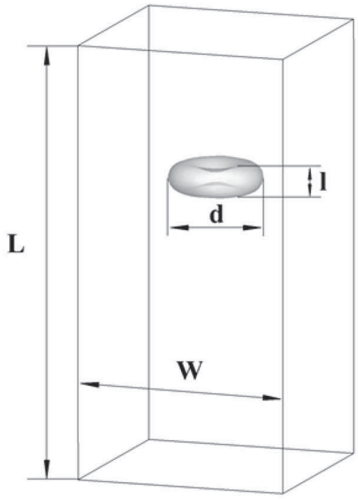

Figure 1: Schematic of the sedimentation of a RBC in a square duct.

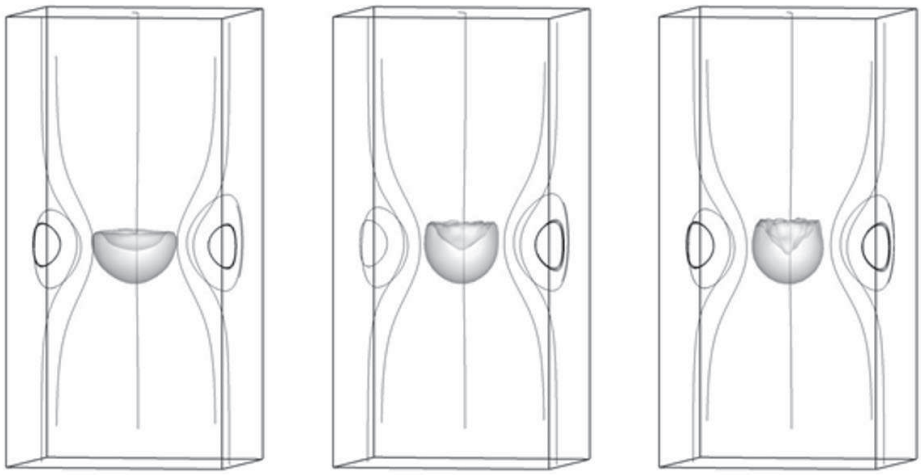

(a) 123 pn (b) 369 pn (c) 615 pn

Figure 2: Streamlines around the RBC & RBC deformation under different external magnetic body forces in a square duct.

First, the effect of the external magnetic body force is investigated. The width of the duct is fixed at $6.36a$. Fig. 2 shows the streamlines around the RBC at different external magnetic body forces when the cell reaches the terminal settling velocity. These streamlines are drawn on the two respective characteristic slice planes. One, defined as Slice 1, is the plane containing the centerline and parallel to one of the duct walls, and the intersected duct walls have the shortest distance to the cell. The other, defined as Slice 2, is the diagonal plane, where the intersected duct walls are furthest from the cell. Fig. 2 illustrates a circulating flow in the lateral region of RBC exists on each slice plane, and it can be deduced that these closed streamlines will form a closed stream-surface with the shape of an annulus. However, we can determine that the size of the circulating region on each slice plane is different. The size of the circulating region on Slice 1 is much smaller than that on Slice 2, and the circulating region on Slice 2 is closer to the RBC than that on Slice 1, indicating that the distance between the cell and duct wall has an important effect on the flow field. The stronger the wall effect is, the more hardly the circulating flow is formed. The corresponding streamlines in different cases start from the same location. As such, the shape of the streamline is similar, and the effect of magnification of the force is not significant.

Fig. 3 illustrates the development of the terminal settling velocity of RBCs with respect to the loads of external force where the velocities are scaled by U_0. The scaled terminal settling velocities are around 0.5. If the undeformed RBC is regarded as a disk, the terminal settling velocity in the infinite flow field is given by:

$$U_T = \frac{3F}{16\pi d\mu_f}, \tag{3.3}$$

where $d = 2.798a$, resulting in $U_T/U_0 = 0.402$, which is close to our computation

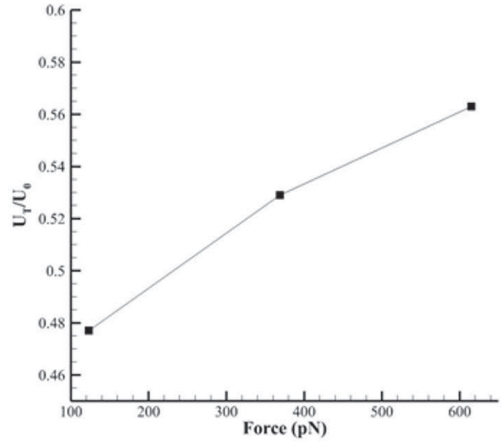

Figure 3: Terminal settling velocity of RBC variations under external forces in a square duct.

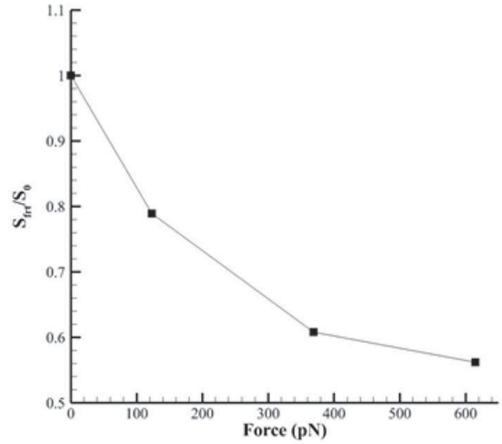

Figure 4: Frontal area of RBC variations under external magnetic body forces in a square duct.

results and provides a brief estimation and validation. As the load increases, the scaled settling velocity increases. If the cell is rigid, the scaled settling velocity should be kept as a constant, disregarding the external force. Hence, Fig. 3 also illustrates the effect of RBCs deformation on the terminal settling velocity. Fig. 4 presents how the frontal area varies with respect to the external load, where the frontal area, S_{frt}, is scaled by the initial area $S_0 = \pi d^2/4$ and d is the diameter of the undeformed RBC. As the external force increases, we find that the lateral length of the cell becomes small, so the frontal area of RBC will decrease (Fig. 4) and result in lower drag. Hence, larger terminal settling velocity is required so that the viscous drag can balance the external magnetic body force.

Usually, the deformation of RBCs in response to an external magnetic body force is

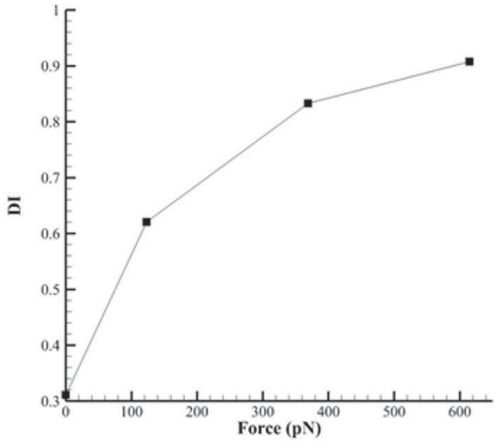

Figure 5: Deformation index of RBC variations under external magnetic body forces in a square duct.

measured by the deformation index (DI) defined as [23]:

$$DI = \frac{l}{d}. \tag{3.4}$$

As shown in Fig. 1, l and d are the length and diameter of a RBC, respectively. In our current study, the configuration is symmetric, and the deformation of RBC is relatively simple. Hence, together with the frontal area, the DI can describe the main character of the deformation.

Fig. 5 shows the variation of the DI of a RBC according to the external magnetic body force. As depicted in Fig. 2, during the sedimentation of RBC, the frontal surface with respect to the sedimentation suffers the largest deformation where the initial concave surface becomes convex. However, the back surface rolls toward the interior of the cell and becomes more concave. This mechanism will elongate the RBC along the direction of the movement. According to the constitutive equations of RBC membrane, the RBCs surface area and volume are constrained to change little during the deformation. When the cell is elongated, the cross size should be reduced to satisfy the volume constraint. The larger the external force, the more the cell is elongated. The transverse size and frontal area are reduced, which is why the DI increases with the magnification of the loads, as shown in Fig. 5.

It should be clarified that although the style of RBC deformation is similar to that in the Poiseuille flow driven by either pressure or body force, the mechanism of deformation is different. In the Poiseuille flow, the flow is active and dominant, but the deformation is passive. The motion of material points on the membrane is determined by the velocity distribution of the flow field. In this current study, the cells deformation is determined by the external magnetic body force. The magnetic body force causes the deformation of the cell and drives the flow. Although the flow also affects the cells shape, the body force is the driving source of the flow and deformation of RBC.

Table 1: Wall effects on the terminal settling velocity and deformation index.

	$W = 4.26a$	$W = 6.38a$
U_T/U_0	0.331	0.529
DI	0.856	0.833
S_{frt}/S_0	0.594	0.608

The effect of the duct wall is studied by varying the ducts width W. Table 1 lists the variations of the scaled terminal settling velocity and the DI due to the change of W with the external body force fixed at 369 pN. From Table 1, we can determine the importance of the wall effect of the duct. On one side, if the settling velocity is the same due to the non-slip boundaries, the existence of the wall will increase the shear rate and exert a retarding effect on the terminal settling velocity. Table 1 also shows that terminal settling velocity is significantly reduced as the duct wall approaches the cell. On the other side, the material particles tend to get forced away from the wall, which is another well-known aspect of wall effect. Because of the symmetric configuration in the present computations, the summation of such an aspect of wall effect is squeezing the cell along the transverse direction so that the lateral size is reduced. Due to the conservation of RBC volume, the cell will be elongated. Although the terminal settling velocity at $W = 4.26a$ is much lower than that at $W = 6.38a$, the DI is larger, and the frontal area is smaller when $W = 4.26a$, indicating that velocity has less effect on deformation. It can be concluded that when the cell is near a wall, the wall effect is as important as the external body force on both the RBC deformation and the translating velocity.

3.2. Modeling the sedimentation of a RBC in a circular pipe

In this section, the RBC is placed in a circular pipe. The sedimentation of a RBC in a circular pipe is investigated and compared to that in a square duct to illustrate another aspect of wall effect: the shape of the cross-section. All of the computational configurations, including the mesh size of the fluid field and RBC membrane, boundary conditions, and material properties, etc., are setup to be the same as described in the previous section except the cross-section shape of the pipe. To facilitate the comparison, the diameter of the pipe cross-section is also set to $6.38a$.

Fig. 6 presents the streamlines around the RBC at different external magnetic body forces when the RBC reaches the terminal settling velocity. Compared to Fig. 2, there is no significant difference to the RBCs shape under the corresponding external magnetic body force. The streamlines are also drawn on the same slice planes defined in the earlier Slice 1 and Slice 2. In this section, because of the symmetric configuration, the flow on Slice 1 and Slice 2 is almost identical. It is evident that the distance from the cell to the wall in a square duct is farther than that in a circular pipe on Slice 2, and the size of the circulating region is larger in the square duct. However, the distance from the cell to the wall in the square duct is the same as that in the circular pipe on Slice 1,

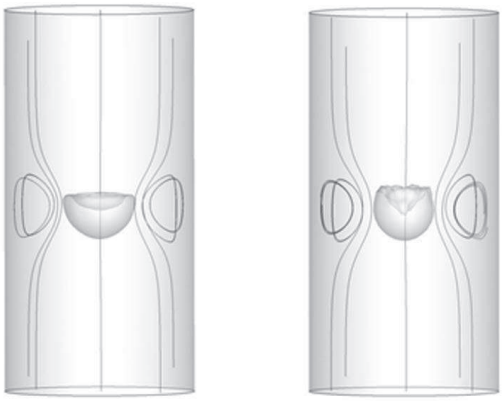

(a) 123 pn (b) 615 pn

Figure 6: Streamlines around the RBC & RBC deformation under different external magnetic body forces in a circular pipe.

and the size of the circulating region is much smaller in the square duct.

Table 2 lists the scaled terminal settling velocities and DIs at the loads of 123 pN and 615 pN, respectively. Table 2 also provides a comparison of corresponding data between the cases in the circular pipe and in the square duct. The variation of the parameters describing the motion and deformation of RBC with respect to the external body force is similar to that in the square duct: the larger the external body force is imposed, the larger the scaled settling velocity and the DI are.

Table 2: Comparison of the wall effect on the terminal settling velocity and deformation index.

	$F = 123\ pn$		$F = 615\ pn$	
	Square duct	Circular pipe	Square duct	Circular pipe
U_T/U_0	0.477	0.429	0.563	0.517
DI	0.620	0.624	0.907	0.915
S_{frt}/S_0	0.789	0.785	0.562	0.559

According to the comparison of the two cases in Table 2, it can be observed that under both loads, the difference on RBC deformation is not obvious when the variations of the DI and the frontal area are less than 1%. The terminal steady shapes of the RBC are almost identical, which is also observed in Fig. 2 and Fig. 6. However, the difference of the scaled settling velocity is much more significant: around 10%. From Table 2, it can be deduced that the terminal settling velocity is more sensitive to the wall effect than the DI and the frontal area.

Furthermore, the effect of the cross-section shape on the RBC actually is the sequence of the two kinds of wall effects noted in the previous section. The retarding effect mainly influences the RBC motion parallel to the wall and reduces the translating velocity of the cell. The repelling effect primarily acts on RBC motion in the normal

direction of the wall. In current symmetric configurations, the repelling effect leads to the squeezing effect on the cell. In the present computation, regarding the shape of the cross-section, the circle is the inscribed circle of the square. Although the perimeter of the square is larger than the circle, the point on the circle is no further than the point on the square to the center. From analyzing the shape of the cross-section and Table 2, it can be concluded that the retarding effect is more sensitive to the distance between the material point and the wall than the repelling effect.

4. Conclusion

In this work, the sedimentation of RBC in a square duct and a circular pipe is investigated. In addition, the flow field and deformation of RBC are investigated. It is observed that the terminal settling velocity increases incrementally with the exerted magnetic body force. The deformation of RBC has a significant effect on the terminal settling velocity due to the change of the frontal area. The larger the exerted magnetic body force, the smaller the frontal area and the larger the RBC deformation become. Deformation amplifies the increment of the terminal settling velocity. The wall effect presents as the retarding effect in the parallel direction of the wall surface, providing additional drag to the cell. In the normal direction of the wall, the wall effect repels the cell away from the wall and, in this current study, presents as the squeezing effect due to the symmetric configuration, which will reduce the frontal area and elongate the cell. The exerted magnetic body force and wall effect play the dominant role in RBC deformation. If the wall is far from the cell, the wall effect will vanish. However, in both cases, the velocity of the flow field is less important with respect to the shape of the cell, which makes it different from the RBC deformation in Poiseuille flow.

Acknowledgments Xing Shi would like to acknowledge support from the National Natural Science Foundation of China (Grant Nos. 10902098, 11372278) and the Fundamental Research Funds of the Central Universities (Program No. 2010QNA40107). Guang Lin would like to acknowledge support from the Applied Mathematics Program within the Department of Energys (DOE) Office of Advanced Scientific Computing Research (ASCR) as part of the Collaboratory on Mathematics for Mesoscopic Modeling of Materials (CM4). The research was performed using Pacific Northwest National Laboratory (PNNL) Institutional Computing, as well as the National Energy Research Scientific Computing Center at Lawrence Berkeley National Laboratory. PNNL is operated by Battelle for the DOE under Contract DE-AC05-76RL01830.

References

[1] Melville, D., Paul, F., Roath, S., Direct magnetic separation of red cells from whole blood, Nature, 1975; 255:706.

[2] Svoboda, J., Separation of red blood cells by magnetic means, J. Magn. Magn. Mater., 2000; 220:103-105.

[3] Tao, R., Huang, K., Reducing blood viscosity with magnetic fields, Phys. Rev. E, 2011; 84:011905.
[4] Fung, Y.C., Biomechanics: Mechanical Properties of Living Tissues, 2nd ed. Springer-Verlag, New York, 1993.
[5] Fung, Y.C., Zweifach, B.W., Microcirculation: Mechanics of blood low in capillaries. Annu. Rev. Fluid Mech., 1971; 3:189-210.
[6] Evans, E.A., New membrane concept applied to the analysis of fluid shear- and micropipette-deformed red blood cells. Biophys. J., 1973; 13(9):941-954.
[7] Skalak, R. Branemark, P.I., Deformation of red blood cells in capillaries. Science, 1969; 164 (3880):717-719.
[8] Secomb, T.W., Skalak, R., Oozkaya, N., Gross, J.F., Flow of axisymmetric red blood cells in narrow capillaries. J. Fluid Mech., 1986; 163:405-423.
[9] Boey, S.K., Boal, D.H., Discher, D.E., Simulations of the erythrocyte cytoskeleton at large deformation. I. Microscopic models. Biophys. J., 1998; 75(3):1573-1583.
[10] Li, J., Dao, M., Lim, C.T., Suresh, S., Spectrin-level modeling of the cytoskeleton and optical tweezers stretching of the erythrocyte. Biophys. J., 2005; 88(5):3707-3719.
[11] Fedosov, D., Caswell, B., Karniadakis, G.E., A multiscale red blood cell model with accurate mechanics, rheology, and dynamics. Biophys. J., 2010; 98(10):2215-2225.
[12] De Hart, J., Peters, G.W.M., Schreurs, P.J.G., Baaijens, F.P.T., A three-dimensional computational analysis of fluidstructure interaction in the aortic valve. J. Biomech., 2003; 36(1):103-112.
[13] Peskin, C.S., Numerical analysis of blood flow in the heart. J. Comput. Phys., 1977; 25:220-252.
[14] Glowinski, R., Pan, T., Périaux, J., A fictitious domain method for external incompressible viscous flow modeled by Navier-Stokes equations. Comput. Method Appl. Mech. Eng., 1994; 112(1-4):133-148.
[15] Liu, Y., Liu, W.K., Rheology of red blood cell aggregation by computer simulation. J. Comput. Phys., 2006; 220(1):139-154.
[16] Yu, Z., A DLM/FD method for fluid/flexible-body interactions. J. Comput. Phys., 2005; 207(1):1-27.
[17] Pan, T.W., Shi, L., Glowinski, R., A DLM/FD/IB Method for Simulating Cell/Cell and Cell/Particle Interaction in Microchannels. Chinese Ann. Math B., 2010; 31(6):975-990.
[18] Shi, X., Lim, S.P., A LBM-DLM/FD method for 3D fluid-structure interactions. J. Comput. Phys., 2007; 226(2):2028-2043.
[19] Chen, S., Doolen, G.D., Lattice Boltzmann method for fluid flows. Annu. Rev. Fluid Mech., 1998; 30:329-364.
[20] Nourgaliev, R.R., Dinh, T.N., Theofanous, T.G., Joseph, D., The lattice Boltzmann equation method: theoretical interpretation, numerics and implications. Int. J. Multiphase Flow, 2003; 29(1):117-169.
[21] X. Shi, G. Lin, J. Zhou, D. Fedosov, A lattice Boltzmann fictitious domain method for modeling red blood cell deformation and multiple-cell hydrodynamic interactions in flow. Int. J. Numer. Meth. Fl., 2013; 72(8):895-911.
[22] Tanimoto, Y., Kakuda1, Y., Influence of strong magnetic field on the sedimentation of red blood cells. J. Phys.: Conf. Ser., 2009; 156:012030.
[23] Tsukada, K., Sekizuka, E., Oshio, C., Direct measurement of erythrocyte deformability in diabetes mellitus with transparent microchannel capillary model and high-speed video camera system. Microvas. Res., 2001; 61(3):231-239.